BEILSTEIN ARCHIVES

This open access document is published as a preprint in the Beilstein Archives with doi: 10.3762/bxiv.2019.104.v1 and is considered to be an early communication for feedback before peer review. Before citing this document, please check if a final, peer-reviewed version has been published in the Beilstein Journal of Nanotechnology.

This document is not formatted, has not undergone copyediting or typesetting, and may contain errors, unsubstantiated scientific claims or preliminary data.

Preprint Title Structural optical and electrical properties of transparent conductive ITO/Al-Ag/ITO multilayer contact

Authors Aliyu K. Isiyaku, Ahmad H. Ali and Nafarizal Nayan

Publication Date 11 Sep 2019

Article Type Full Research Paper

ORCID® iDs Aliyu K. Isiyaku - https://orcid.org/0000-0002-7266-3298

License and Terms: This document is copyright 2019 the Author(s); licensee Beilstein-Institut.

This is an open access publication under the terms of the Creative Commons Attribution License (http://creativecommons.org/licenses/by/4.0). Please note that the reuse, redistribution and reproduction in particular requires that the author(s) and source are credited.
The license is subject to the Beilstein Archives terms and conditions: https://www.beilstein-archives.org/xiv/terms.
The definitive version of this work can be found at: doi: https://doi.org/10.3762/bxiv.2019.104.v1

Structural optical and electrical properties of transparent conductive ITO/Al-Ag/ITO multilayer contact

Aliyu Kabiru Isiyaku[a,b*] Ahmad Hadi Ali[a], Nafarizal Nayan[c]

[a*] Optical Fiber Laser Technology Group, Department of Physics and Chemistry, Faculty of Applied Sciences and Technology Pagoh Educational Hub, University Tun Hussein Onn Malaysia, 84600 Pagoh, Johor Malaysia.

[b] Department of Physics, Faculty of Science, Kaduna State University, P.M.B 2339, Kaduna State, Nigeria.

[c] Microelectronic and Nanotechnology Shamsuddin Research Centre (MiNT-SRC), Universiti Tun Hussein Onn Malaysia.

Abstract

Developing a new design and structure of transparent conductive oxides (TCO) materials to improve performance in optoelectronic devices are important and quite challenging. Microstructural, optical and electrical properties of sandwiched Al-Ag metals interlayer between top and bottom ITO layers (ITO/Al-Ag/ITO) have been investigated. The multilayer ITO/Al-Ag/ITO (IAAI) films were prepared using RF and DC magnetron sputtering method. Post annealing treatment at 400°C was conducted on IAAI and ITO (for reference) films in air. X-ray diffraction measurements show that the insertion of Al-Ag intermediate bilayer led to the crystallization of Ag interlayer even at as-deposited stage. Peaks intensities at ITO (222), Ag (111) and Al (200) crystal plane were observed after annealing treatment, indicating an enhancement in crystallinity of the IAAI film. The post-annealed IAAI film reveals a continuous and smooth surface roughness with improved growth in grain size as examined by atomic force microscopy (AFM) and field emission scanning electron microscopic (FESEM) respectively. Comparing the optoelectronic properties of IAAI film with single ITO film, the annealed IAAI film exhibited a remarkable improvement in optical transmittance (86.1%) with a very low sheet resistance of 2.93 Ω/sq as measured by UV-Vis spectrophotometer and four-point probe method. The carrier concentration increased more than double when Al-Ag layer was inserted between the ITO layers as determined by Hall Effect measurements. The under layer Al film helps to halts the Ag film agglomeration and oxidation which subsequently enhances the stability of IAAI multilayer film. The performance of IAAI contact has been found to be high at 76.4×10^{-3} Ω compares to single ITO (69.4×10^{-3}) contact as calculated by the figure of merit (FOM).

Keywords: figure of merit; ITO; multilayer structure; post–annealing treatment; RF sputtering.

Introduction

Presently transparent conducting oxides (TCO) thin films have been receiving much attention due to their massive contribution as a contact in several optoelectronic devices such as LED[1], solar cell [2] and flat panel display[3]. Indium tin oxide (ITO) is the most considered TCO for industrial and laboratory applications due to its excellent optical and electrical properties [4,5]. It is a wide band gap material (~3.6 - 4.0 eV) with low electrical resistivity and because of those factors, it dominates the optoelectronic market. ITO constitutes a rare and expensive indium metal which reflect in the market value of the material[6]. Hence, the need for reduction of ITO consumption is necessary for friendly market value. Adjustment of ITO film to a small thickness could result in high optical transmittance in the visible region but resistivity increases which is an issue [4,7-8]. Therefore, the search for new material design and structures of ITO based films to enhance performance in optoelectronic devices is of paramount importance. Inclusion of metal thin film between the top and bottom of ITO layers (multilayer structure) has been explored recently for efficient photoelectric devices[7]. As reported, the multilayer structure not only improves the conductivity property of the contact but also make the device cost-effective since indium metal consumption is reduced[9-11]. The insertion of metal layer reduces the transparency of the ITO due to opaqueness nature of the metal, but selecting an optimum metal thickness can effectively decrease the reflection from the metal films and hence enhances the transmittance. Furthermore, it gives room for selective transparency in the visible region of the spectrum [9,12-13]. However, it is observed that the quality of both the metal and ITO layers determines the optical and electrical performance of the multilayer structures[4].

Embedding metal thin film in-between ITO layers couple with annealing process enhances the photo-responses and rectification properties of the ITO device. Single or double metal thin films of either Ag, Al, Ti, Au, Cr, or Ni have been used to embed ITO layers for improving performance[4, 8,14-17]. Free electrons in metal inserted ITO materials speed up the separated charge carriers and hence gear up the light transport from lower to the upper part when the light is incident on the device[9]. Al films good adhesion, low resistivity, non-oxidation and corrosion properties are quite impressive and as such is suitable for optical and electronic device applications [18-20]. The low resistivity and high transmittance (compared to other metals) in the visible region of Ag thin films at room temperature are key properties

that attracted the widely use of Ag layer in ITO multilayer contacts [21-24]. In spite of the magnificent effects of annealing process on ITO based multilayer, deposited Ag thin films agglomerate upon annealing due to low adhesion and easy wandering of Ag atoms to the surface which degrade the properties of the film [25]. This issue can be overcome by embedding thin metal film of any of Al, Au, Pd, or Cr etc., in Ag film due to their adhesion property [4,25-26].

Optical and electrical properties of ITO films are enhanced by post-deposition annealing especially at high temperature [7]. Gulen et al. [27] exposed single ITO films deposited by sputtering to heat treatments at different temperatures 100ºC-700°C. Effective improvement in microstructural, optical and electrical properties of the film annealed at 400 °C was observed. Similarly, a significant enhancement in optoelectronic properties of ITO/Ag(Cr)/ITO multilayer was achieved by film annealed at 500°C[4]. Further treatments beyond 500°C resulted in the degradation of films structure due to the appearance of metallic nanoparticle on the multilayer surface [4, 28]. Furthermore, post-annealing at 200 °C was found to be remarkable for 5.07 nm intermediate Al films with an estimation of 12.28×10^{-4} Ω^{-1} figure of merit (FOM) as obtained by Cho et al., [29]. Rapid thermal annealing conducted on ITO/Ag/ITO films by Joeng et al., [28] indicates a good improvement in transmittance for film annealed at 300°C and lowest sheet resistance and resistivity was obtained by film annealed at 500°C but with reduced optical transmittance. Also in a similar case, a durability test of ITO sandwich Ag-alloy interlayer electrode against heat treatment was carried out by Roh et al. [30] at 450ºC. Ag films appreciable durability and stability was observed. In the present work, structural, optical and electrical properties of Al-Ag bilayer inserting ITO layers (ITO/Al-Ag/ITO) are highlighted. Moreover, post-annealing treatment was conducted at 400ºC on both the ITO/Al-Ag/ITO (IAAI) multilayer film and grown single ITO film for comparison.

Results and discussion

Figure 1 shows the X-ray diffraction (XRD) patterns for as-deposited and annealed IAAI multilayer films. The as-deposited film shows an amorphous structure for top ITO layer with a strong Ag diffraction peak at (111) direction, showing that, Ag intermediate layer is present in a crystalline phase as also obtained in the work of Kim et al.[31]. The IAAI film becomes polycrystalline upon annealing at 400ºC. Strong peak intensities at (222), Ag (111) and (440) crystal directions were observed after post-annealing treatment. The appearance of diffraction peaks of ITO (222), Ag (111) and Al (200) intensities on annealed film indicates a crystalline

enhancement in the film. The diffraction peaks of In_2O_3 appears to be dominant without tracing any of SnO_2, Sn or SnO characteristics peaks.

Upon deposition of the IAAI films, the kinetic energies (K.E) of sputtered atoms arriving at the substrates are low and hence the amorphous structure. But it can be noted that the K.E of the arriving sputtered Ag particle atoms is a bit higher and therefore crystallized at the as-deposited level. Furthermore, on annealing, the sputtered surface adatoms gain additional K.E after relieving itself with some stress which also led to an increase in adatoms mobility. This process enables grain growth and crystallization and similar findings were reported by some researchers [32-34]. Similarly, grain sizes of as-deposited and annealed IAAI films were calculated using Debye-Scherer equation,

$$D = {}^{0.9\lambda}/_{\beta cos\emptyset} \tag{1}$$

Where λ is the X-ray wavelength of the Cu-Kα radiation (1.5406 Å), β is the corrected full width at half-maxima (FWHM) and Ø is the Bragg angle. The calculated grain sizes are 51.6 nm for as-deposited IAAI film and 68.9 nm for annealed IAAI film.

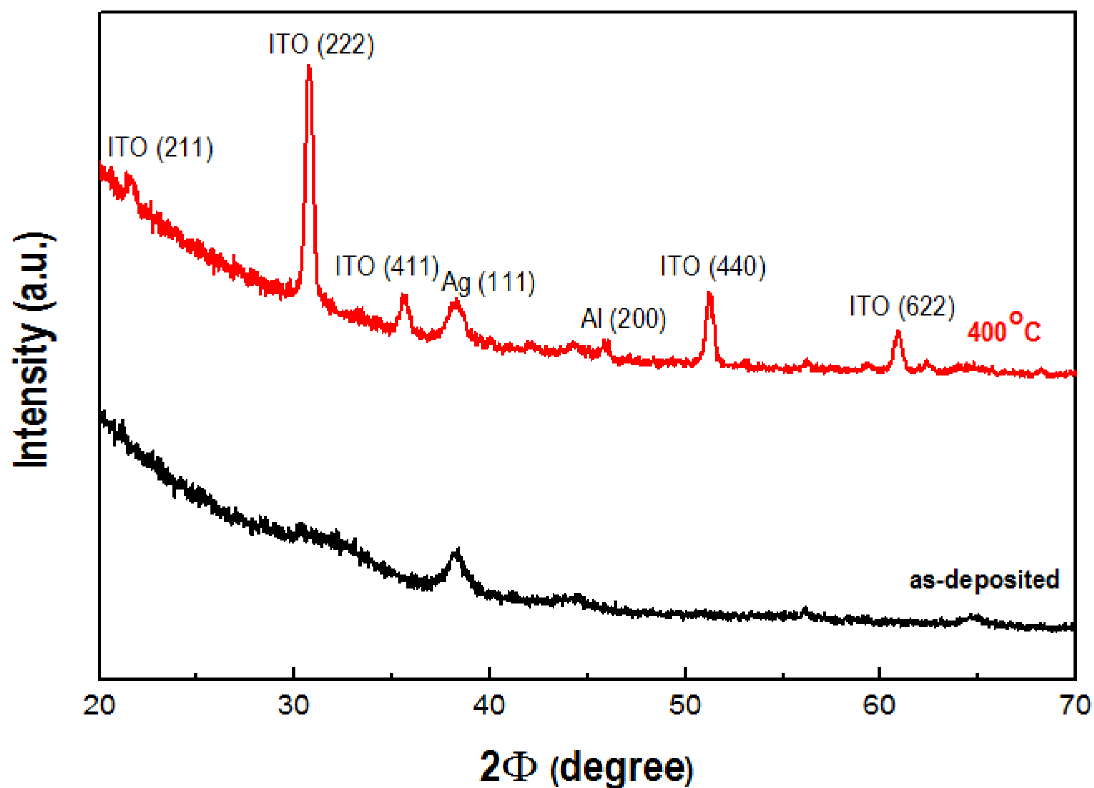

Figure 1: XRD spectra for as-deposited and annealed IAAI films.

The elemental composition (weight %) of the IAAI films on Si substrate scanned by energy-dispersive x-ray spectroscopy (EDXS) is displayed in Table 1. Reduction in weight per cent of nitrogen N and oxygen O was observed after annealing treatment. Whereas, an increase in weight per cent of the metal and semiconductor materials including Al, Ag, In, Sn and Si were also observed after annealing process with Si material showing the highest elemental composition. The large weight composition of Si is due to its position as the base material. Moreover, Sn exhibited a low composition because it serves as a dopant element to ITO. The low composition was additionally observed in Al material which is attributed to its very thin layer. The scanned elemental distribution for both the as-deposited and annealed IAAI films are shown in Figure 2 (a and b).

Table 1: Elemental composition in weight % of the IAAI films on the silicon substrate

Elemental (weight)	N	O	Al	Ag	Si	In	Sn
As-deposited IAAI	3.41	12.51	0.51	11.01	49.01	22.09	1.46
Annealed IAAI	2.11	11.01	0.57	11.50	50.50	22.32	1.99

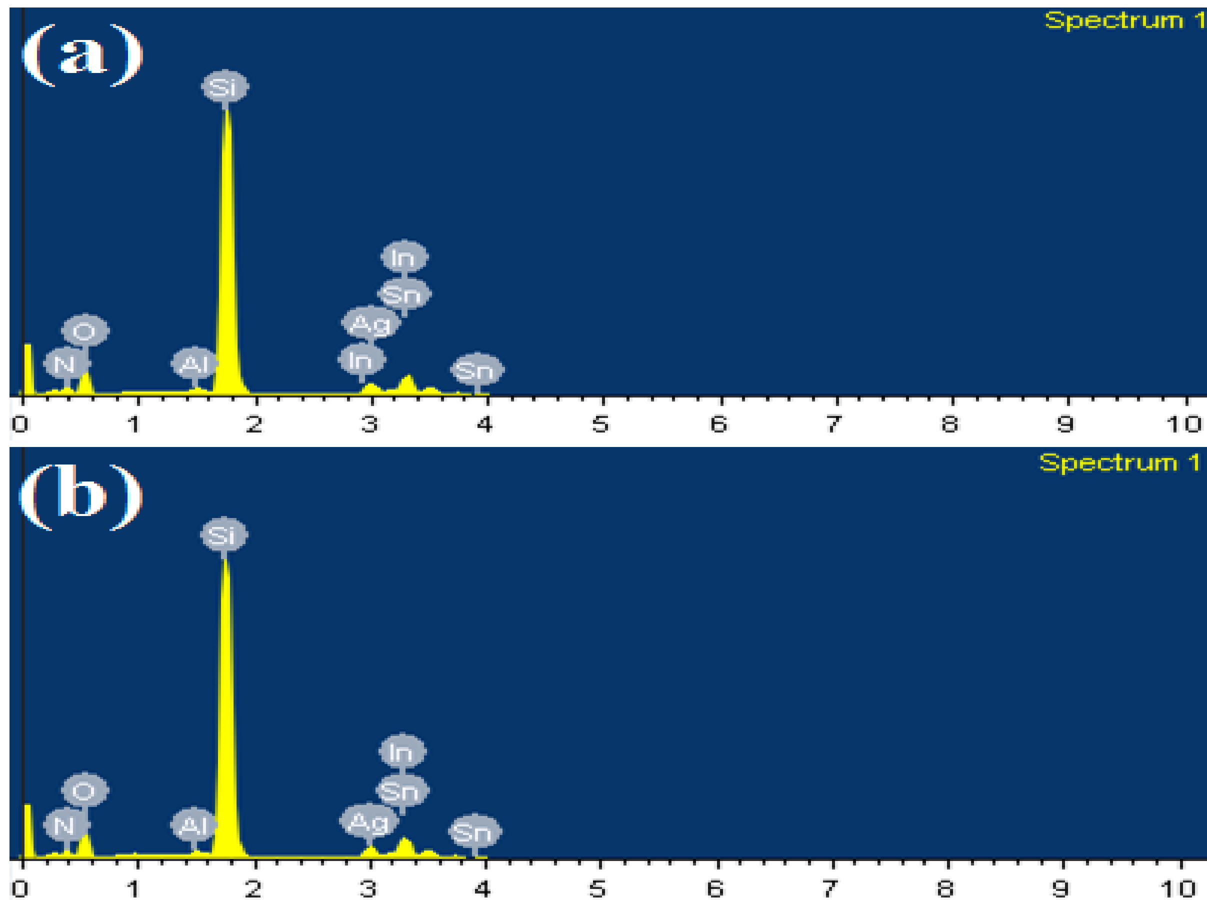

Figure 2: EDXS properties of (a) as-deposited IAAI (b) annealed IAAI

Surface morphology of the IAAI and ITO films was studied using atomic force microscope (AFM) system scanned over an area 1 µm x 1 µm as shown in Figure 3 (three dimensional, (3D) images). Smooth surface roughness with an increased root means square (Rrms) and average roughness (Ra) values for both IAAI and ITO films after post-annealing treatment were observed. As determined by Nanoscope Analysis, average grain size increased from 53.53 nm (as-deposited) to 60.03 nm (annealed) for IAAI films and 27.59 nm (as-deposited) to 31.18 nm (annealed) for single ITO films. The large grain size of IAAI films narrows the grain boundary and reduces the scattering effect within the grain boundary and hence the smoother. The reduction in grain boundary scattering paves the way for improve carrier mobility thereby boosting the films electrical conductivity.

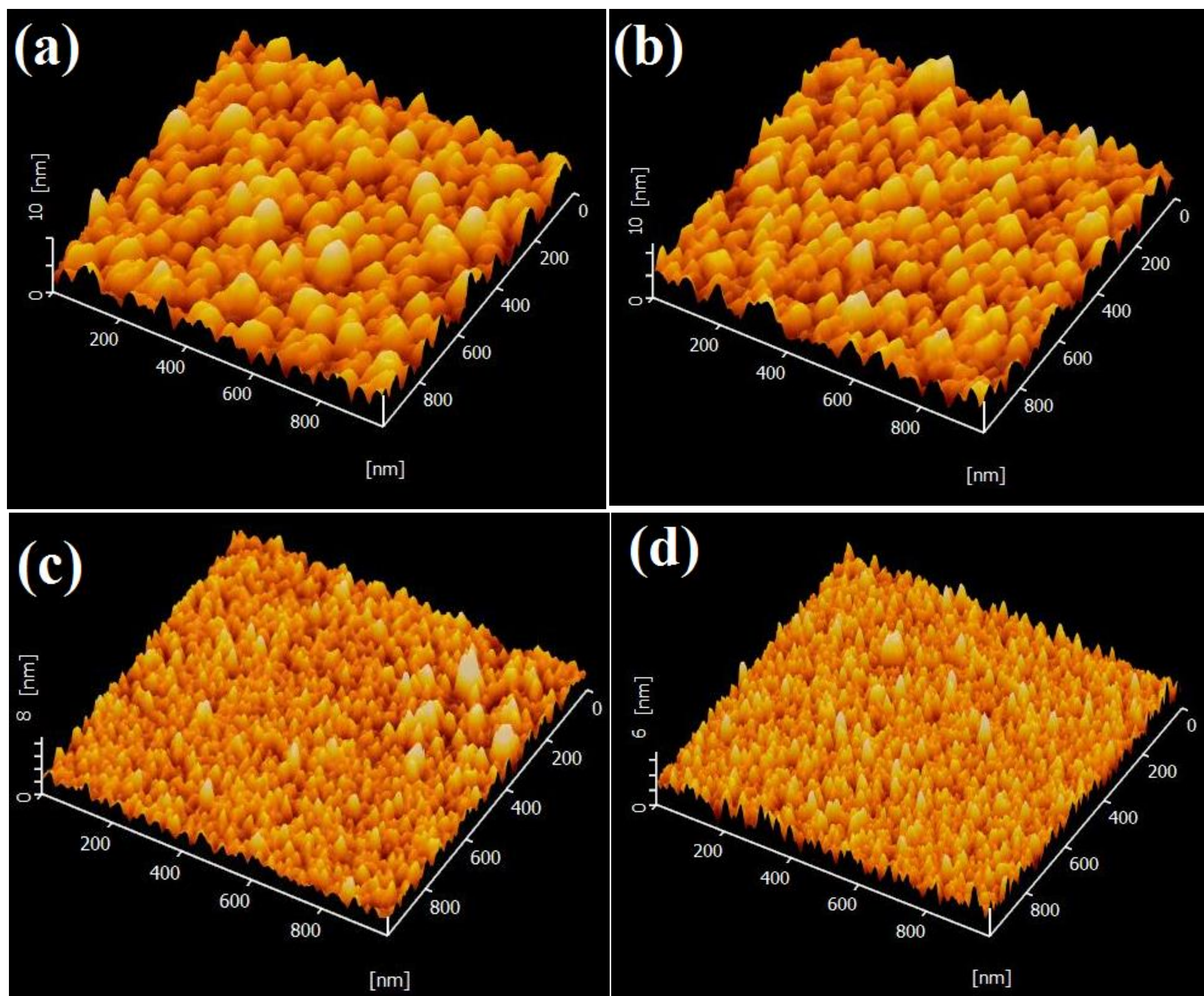

Figure 3: AFM 3D images for (a) as-deposited IAAI film (b) annealed IAAI film (c) as-deposited ITO film and (d) annealed ITO film.

Additionally, surface morphology of the IAAI and ITO films were further analysed by field emission scanning electron microscopic (FESEM) technique using 5.0 kV voltage and 100000x magnification. Figure 4 shows FESEM images of the as-deposited and annealed IAAI and ITO films deposited by a sputtering method. All the as-deposited IAAI and ITO films show a smooth and continuous surface with small grains and dense particles (for IAAI film) evenly distributed. The films surface become smoother and the grain sizes increased after annealing treatment with the IAAI film exhibiting larger grain sizes. Island formation or agglomeration Al-Ag metal films on the surface of the annealed IAAI film was not significant to warrant unwanted microstructural changes and hence, IAAI is said to be stable at this temperature. The films surface roughness results by FESEM and AFM techniques are in good agreement.

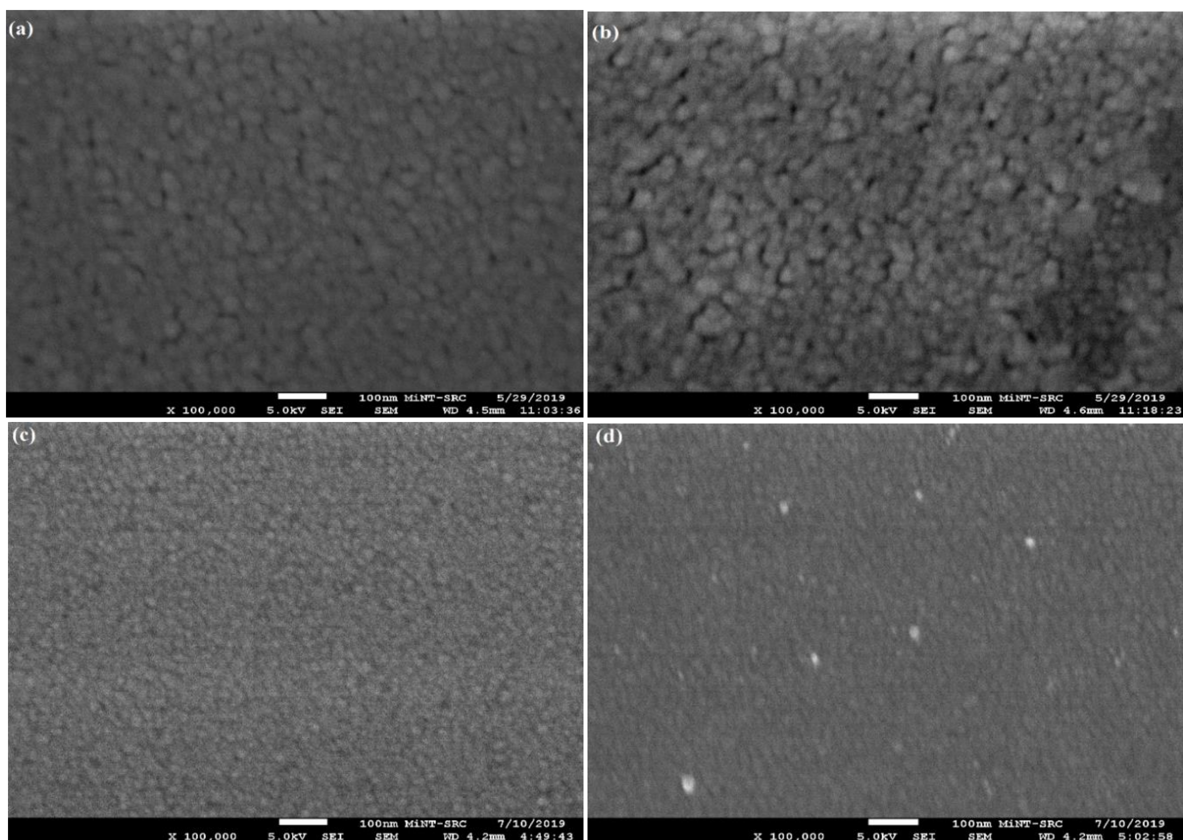

Figure 4: FESEM images of (a) as-deposited IAAI (b) annealed IAAI (c) as-deposited ITO (d) annealed ITO.

The optical characteristics of the as-deposited and annealed IAAI and ITO films as measured by ultraviolet-visible spectrophotometer (UV-vis) is shown in Figure 5. It can be seen, that the annealed IAAI and ITO films show a significant increase in optical transmittance. The post annealed IAAI indicates transmittance of~86.1 % in the visible range. The increase in transmittance is attributed to the improvement of the metals interlayer crystallinity (after annealed) which resulted in minimum light

scattering from the metals thin films [28-30]. Besides, the post-annealing treatment has successfully able to reduce the defects responsible for light scattering and hence the enhancement in structural ordering and consequently the transmittance [4, 35]. The enhanced structural ordering decreases the electron scattering from the grain boundaries and impurities. This can lead to increase in the effective charge carrier conduction. Although, the annealed ITO film at this thickness shows better transmittance characteristics at~96 %, but that comes with an increasing resistivity which is an issue [32, 36]. It can be observed in Figure 5, that the transmittance spectra of the annealed IAAI shifted toward shorter wavelength of the spectrum indicating a blue shift in the transmittance. The increased in ITO film carrier concentration is responsible for the blue shift and this can be clearly explained by the Burstein-Moss shift model[9, 37].

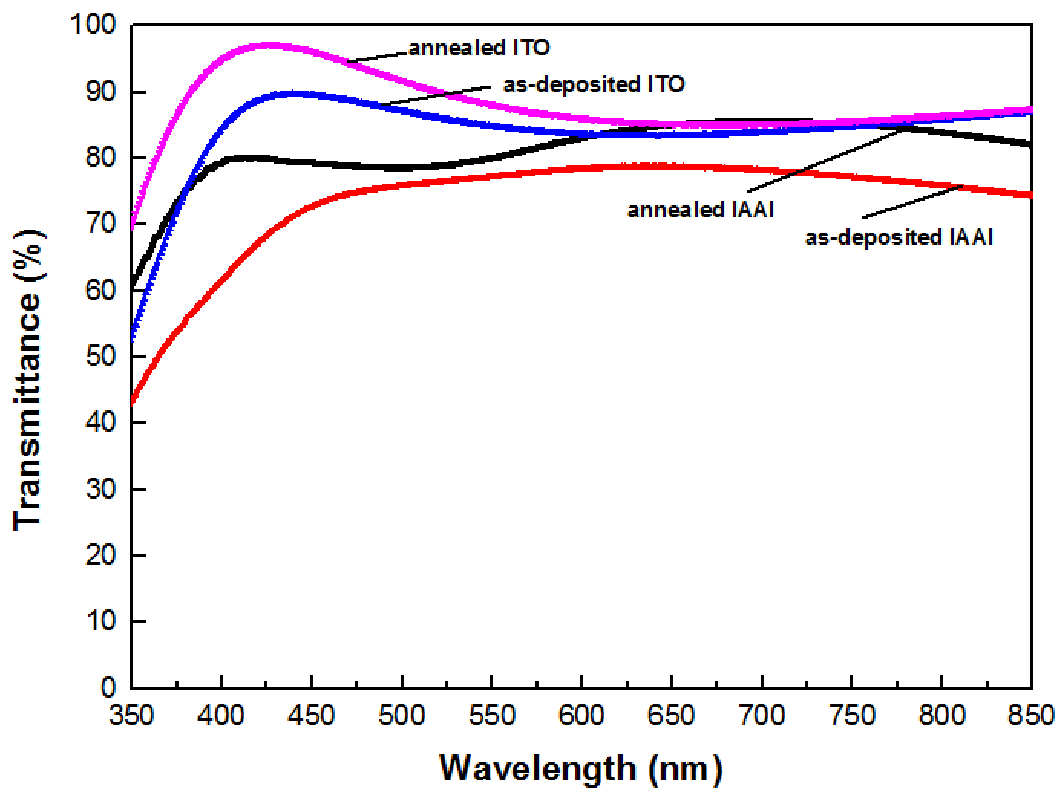

Figure 5: Optical transmittance of as-deposited and annealed IAAI and ITO films.

Electrical properties of IAAI and ITO films from four-point probe and Hall measurements systems were displayed in Table 1 for comparison. Sheet resistance and resistivity of IAAI film are shown to be lower compared to annealed ITO film and further decreases upon annealing at 400^0C in air. The decrease can be attributed to the inclusion of highly conductive (low resistivity) metal layers. Even though metal layers inclusion tends to decrease the transmittance

of the film, the conduction of heat treatment at high temperature narrows the transparency-conductivity trade-off by reducing the film structural defects. Similarly, considering the multilayer structure of IAAI film, it is sheet resistance can be expressed as [29];

$$\frac{1}{R_{sT1}} = \left(\frac{1}{R_{Al}} + \frac{1}{R_{Ag}}\right) + \frac{2}{R_{sITO}} \quad (2)$$

where R_{sT1} is the total sheet resistance of IAAI films, $\left(\frac{1}{R_{Al}} + \frac{1}{R_{Ag}}\right)$ represent the sum of sheet resistant of Al and Ag films, while $\frac{2}{R_{sITO}}$ is the sheet resistance for combined top and bottom ITO thin films.

Lowest sheet resistance and resistivity values of 2.93 Ω/sq and 2.64×10^{-5} were obtained by the annealed IAAI film as indicated in Table 1. Generally, one can say that the inclusion of low resistivity metals thin films, coupled with a reduction in grain boundary scattering that leads to strong film crystallization after post-annealing is responsible for the large reduction in both the sheet resistance and resistivity. The carrier concentration and mobility of IAAI film are relatively higher than the ITO film. The IAAI carrier concentration increased from 6.2×10^{-21} to 8.9×10^{-21} cm^{-3} after post-annealing treatment. Likewise, the carrier mobility increased significantly to~ 30.2 $cm^2V^{-1}s^{-1}$ from~ 22.5 cm^2 $V^{-1}s^{-1}$ (for as-deposited IAAI film). Similar findings were reported by Meshram et al. [4], Kumar et al.[9] and Ali et al.[34] Such that increased in carrier concentration is attributed to grain growth and decreased in scattering mechanism.

Table 2: Comparison of electrical resistivity (Ω cm), sheet resistance (Ω/sq), carrier concentration (cm^3), and carrier mobility (cm^2/Vs) of as-deposited and annealed ITO and IAAI multilayer films.

Factors	as-deposited ITO	annealed ITO	as-deposited IAAI	annealed IAAI
Resistivity (Ω cm)	1.64×10^{-4}	1.52×10^{-4}	8.12×10^{-5}	2.64×10^{-5}
Sheet resistance (Ω/sq)	18.2	9.34	8.12	2.93
Carrier concentration (cm^{-3})	2.01×10^{21}	2.58×10^{21}	6.2×10^{21}	8.9×10^{21}
Mobility (cm^2/Vs)	2.75	5.51	22.5	30.2

The quality of any ITO based film is perfected by high optical transmittance T_{opt} and low sheet resistance R_s. As shown in equation 3, the performance of IAAI multilayer and ITO films were determined using a figure of merit (FOM) developed by Haacke, [38],

$$FOM = \frac{T^{10}}{R_S} \tag{3}$$

Optical transmittance and electrical conductivity properties of IAAI film contact are greatly enhanced as determined by FOM after post-annealing treatment. Figure 6 shows the transmittance peaks and FOM as a function of as-deposited and annealed IAAI multilayer and ITO films. Although ITO film FOM value is higher at as-deposited phase and upon annealing, the IAAI film rose to $76.4 \times 10^{-3}\ \Omega^{-1}$ as against $71.92 \times 10^{-3}\ \Omega^{-1}$ for annealed ITO film. The FOM improvement is as a result of concurrent optical transmittance and conductivity enhancement[4]. It can conclude that the combined Ag and Al metals film couple with the annealing process at $400\,^{0}$C have significantly improved the performance of the multilayer film as determined by FOM. This is due to the rapid reduction in sheet resistance accompanied by the enhanced optical transmittances.

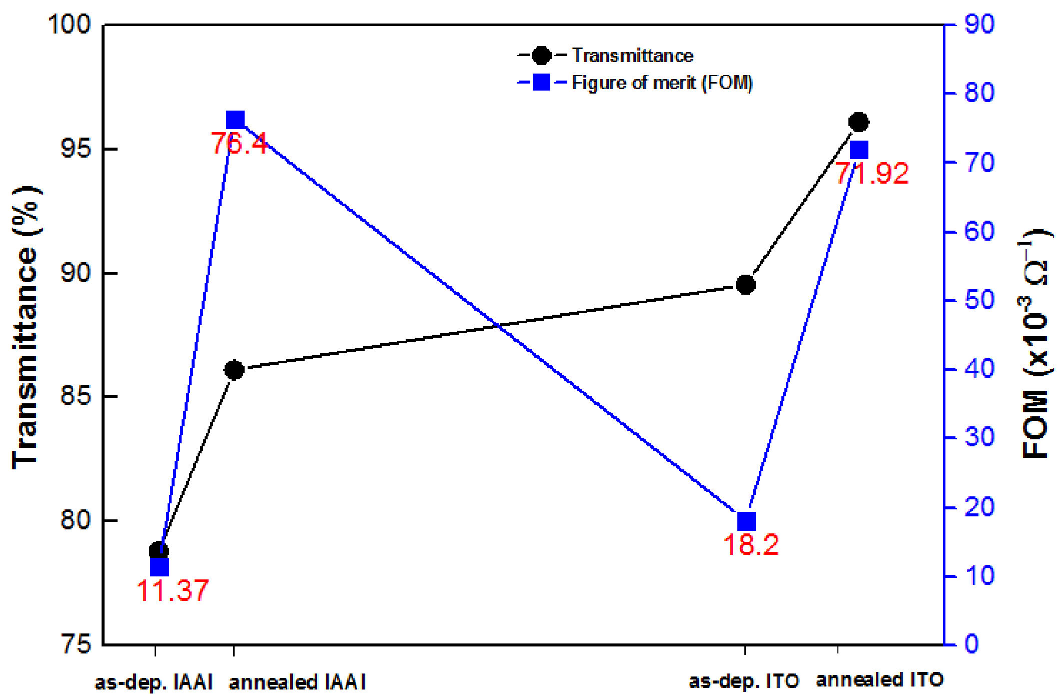

Figure 4: Transmittance and FOM of as-deposited and annealed IAAI multilayer and ITO films.

Conclusion

The multilayer structure of ITO/Al-Ag/ITO (IAAI) film was deposited by RF and DC magnetron sputtering systems at room temperature respectively. Al-Ag bilayer inclusion couple with post-annealing treatment at 400°C significantly enhanced the microstructural, optical and electrical properties of the multilayer film. High optical transmittance of 86.1 % at 450 nm wavelength with a low sheet resistance of 2.93 Ω/sq was obtained for annealed IAAI film. According to figure of merit, it is clear that the annealed IAAI film ($76.4 \times 10^{-3}\ \Omega^{-1}$) exhibited better performance as a transparent contact compared to single ITO film ($71.9 \times 10^{-3}\ \Omega^{-1}$). The improvement in IAAI film optoelectronic properties is aided by the film crystallization after post-annealing treatment. Furthermore, the IAAI larger grain size and smooth surface roughness assist in enhancing the optical and electrical properties.

Experimental

Materials

A commercial $In_2O_3:SnO_3$ (ITO) target of 90:10 weight ratio was used for ITO films deposition. Aluminium (Al) and silver (Ag) targets of 99.999 per cent purity and commercially prepared were purchased and used for the deposition of Al-Ag interlayer between top and bottom of ITO layers. In addition, silicon (Si) wafers of [(100), n-type, phosphorous, 1-10 Ω cm and 525+/-25 microns] orientation together with commercial soda-lime glass (for optical measurements) were used as substrates or based materials. Decon90 glass cleaner was used for glass substrates cleansing.

Thin films preparation

SNTEK Korea model of magnetron sputtering system with a dual sputtering source of radio frequency (RF) and direct current (DC) that comprises the main deposition chamber (15.7 inches in height and 23.6 inches in diameter) was used for the thin films preparation. The top and bottom ITO layers were deposited using RF sputtering while DC sputtering was applied for the Al-Ag bilayer metals thin films deposition. Prior to the deposition, Si substrates were heated in acetone at 55°C for 5 minutes, rinsed in isopropanol and de-ionized water respectively. Similarly, glass substrates were cleaned using Decon90 glass cleaner, and then rinsed in de-ionized water. Both the Si and glass substrates were afterwards dried in N_2 gas atmosphere. Initially, the chamber was evacuated to 6.5×10^{-6} Torr after which the bottom ITO layer was deposited using RF power of 120 W, with 5.2 mTorr working pressure and 50 sccm

Ar gas flow. Before, ITO top layer deposition (same parameters with bottom ITO layer), Al and Ag films were deposited one after the other using DC sputtering source with the following sputtering parameters; DC power of 100 W, 5.2 mTorr working pressure and 100 sccm Ar gas flow for Al film, also a DC power of 100 W, with 4.9 mTorr working pressure and 100 sccm Ar flow was set for Ag film deposition. The deposition process for all the layers was carried out at room temperature with target-to-substrate distance at 7 cm.

Filmetrics F20 thickness measurements

Optical reflectometer Filmetrics F20 system was used to measure all the deposited films thicknesses using a Filmetrics thin film analyser F20 model. Each of the deposited thin films of ITO, Al and Ag were measured separately. For each film, separate structure on Si was set in the FILMeasure software on the computer and all the measurements took place in air environment. Initially, the baseline measurement was conducted before each film thickness measurement was carried out and at least 97.4% of goodness fit was achieved.

Furnace annealing treatment

Carbolite electric furnace was used for the annealing treatments of the prepared thin films samples at 400ºC without the introduction of any gas. In this annealing experiment, prior to temperature settings, the condition of the carbolite furnace was met at room temperature. After the temperature settings, the temperature ramp at 10°C per minutes and when it reached 400°C, it was then allowed to stabilize for 5 minutes before turning down the temperature back to initial room temperature.

Structural analyses of the thin films

The structural properties (phase composition) of the as-deposited and annealed IAAI films were determined using X-ray diffraction (XRD) technique. The PANalytic XPERT-PRO MPD X-ray diffractometer model was used with Cu $K\alpha_1$ (λ = 1.540598 Å) radiation as the excitation source, 40 kV working voltage and 30 mA of filament current. In this experiment, the phase analyses XRD microscope with Cu $K\alpha_1$ (λ = 0.15406 nm) radiation was operated at a range 15-90° of 2 Theta degree. Debye-Scherer equation was used to calculate the crystallites (grain) size after analysing the data obtained from the XRD results.

Elemental composition analyses

Elemental characteristics of the as-deposited and annealed IAAI multilayer films were investigated using energy dispersive x-ray spectroscopy (EDXS). FESEM JEOL JSM-7600F-SM17600053, Japan, equipped with an energy dispersive X-ray spectrometer EDS, OXFORD X-MAX, Energy 200 premium the UK model was used to analyse the elemental composition in weight of the thin films deposited on silicon substrate. The IAAI thin films on silicon substrate were scanned by EDXS tool to generate the elemental composition of the films.

Morphological analyses by Atomic force microscopic

One of the important techniques employed in the analyses of the thin films surface morphology is atomic force microscopic (AFM) and it was used during this experiment. AFM Standard Operation AFM5010 Hitachi model was used to examine the films surface morphology. Root mean square R_q and average R_a roughness plus grain size morphological analyses were carried out using AFM (tapping mode) tool and Nanoscope Analyses software accordingly. All the films were scanned over an area of 1 μm x 1 μm respectively.

Field emission scanning electron microscopic analyses

Surface morphology of the prepared thin films was further studied using field emission scanning electron microscopic (FESEM) technique. FESEM JEOL JSM-7600F- SM17600053, Japan) equipped with an energy dispersive X-ray spectrometer EDS, OXFORD X-MAX, Energy 200 premium the UK was engaged in this experiment. The morphological analyses of the IAAI and ITO films samples conducted by FESEM were performed using 5.0 kV voltage and 100,000 x magnifications.

Optical transmittance analyses

Optical transmittance analyses were carried using Shimadzu UV-3101 PC Ultraviolet-visible (UV-visible) double-beam spectrophotometer model in the range 300 – 700 nm wavelength. The IAAI films deposited on glass substrates were used and prior to optical measurements, background (baseline) measurement was performed using 2 non-doped soda-lime glasses placed at the 2 adjacent samples holder.

Electrical analyses by four-point probe

Electrical properties analyses that involve the measurements of electrical resistivity and sheet resistance of the prepared thin films were performed by four-point probe system. Pro 4 Lucab Lab model was used. The electrical resistance of the samples was determined at room temperature with a four-point probe electrical tester with respect to film thickness (measured) and supply current (4 mA). The results obtained are an accumulated average of the measurements.

Hall Effect measurements analyses

Further studies on electrical properties in terms of carrier mobility and carrier concentration were implemented using Hall Effect measurement system. During this experiment, the maximum voltage and current were set at 20 V and 20 mA respectively using Vander Pauw type method by employing a four-point probe situated around the sample perimeter. All the samples underwent Ohmic contact measurements at room temperature, before Hall mobility and carrier concentration measurements.

Acknowledgements

The support from Universiti Tun Hussein Onn Malaysia, Ministry of Higher Education Malaysia and Kaduna State University, Nigeria are gratefully acknowledged. This research was partially funded by the Fundamental Research Grant Scheme FRGS (Vot. No 1600) and Incentive Grant Scheme for Publication IGSP (U670).

References

[1] Shengjun, Z.; Bin, C.; Sheng, L.; and Han, D. *Opt. Laser Technol.*, **2012**, 44, 2302–2305.

[2] Balestrieri, M.; Pysch, D.; Becker, J. P.; Hermle, M.; Warta, W.; and Glunz, S.W. *Sol. Energy Mater. Sol. Cells*, **2011**, 95, 2390–2399.

[3] Indluru, A.; and Alford, T. L. *J. Appl. Phys.*, **2009**, 105, 123528.

[4] Meshram, N.; Loka, C.; Park, K. R.; and Lee, K. S. *Mater. Lett.*, **2015**, 145, 120–124.

[5] Lippens, P.; Buchel, M.; Chiu, D.; and Szepesi, C. *Thin Solid Films*, **2013**, 532, 94–97.

[6] Song, S. *et al.*,. *Vacuum*, **2009**, 83, 1091–1094.

[7] Guillén, C.; and Herrero, J. *Thin Solid Films*, **2011,** 520, 1–17.

[8] Chakaroun, M.; Lucas, B.; Ratier, B.; and Aldissi, M. *Energy Procedia*, **2011**, 31, 102–109.

[9] Kumar, M. D.; Park, Y.C.; and Kim, J. *Superlattices Microstruct.*, **2015**, 82, 499–506.

[10] Guillén, C.; and Herrero, J. *Sol. Energy Mater. Sol. Cells*, **2008,** 92, 938–941.

[11] Bou, A. *et al.*,. *J. Phys. D. Appl. Phys.*, **2015**, 48, 205102.

[12] Lin, T. C.; Huang, W. C.; and Tsai, F. C. *Microelectron. Eng.*, **2017**, 167, 85–89.

[13] Ghosh, D. S. Switzerland: Springer, **2013**, 11–33.

[14] Ali, A. H.; Hassan, Z.; and Shuhaimi, A. *J. Alloys Compd.*, **2016**, 681, 186–190.

[15] Yang Li, Q. Y.; Wang, Li.; Chang, C.; Duan, L. *Chinese Sci. Bull.*, **2004**, 49, 1328–1331.

[16] Kim, D. *Appl. Surf. Sci.*, **2010**, 256, 1774–1777.

[17] Lin, Y. C.; Chang, S. J.; Kuo, C. W.; and Chen, S. C. *Solid. State. Electron.*, **2003**, 47, 849–853.

[18] Muralidhar S. M.; Vijaya, G.; Krupashankara, M. S.; Sridhara, B. K.; and Shridhar, T. N. *Mater. Today Proc.*, **2018**, 5, 2696–2704.

[19] Mwema, F. M.; Oladijo, O. P.; Akinlabi, S. A.; and Akinlabi, E. T. *J. Alloys Compd.*, **2018**, 747, 306–323.

[20] Quintana, P.; Oliva, A.; Ceh, O.; and Corona, J. E. *Superf. y vacío*, **1999**, 12, 280–282.

[21] Isiyaku, A. K.; Ali, A. H.; and Fauziyyah Ramly, N. *Mater. Today Proc.*, **2019**, 7, 692–696.

[22] Chiu, P. K.; Chen, W.; Chen, H. P.; Hsiao, C. N.; and Yang, J. R. in *The 4th IEEE International NanoElectronics Conference*, **2011**, 1–2.

[23] Jeong, J. A; Kim, H. K.; and Yi, M. S. *Appl. Phys. Lett.*, **2008**, 93, 1–4.

[24] Park, Y.-S. *et al.*,. *J. Electrochem. Soc.*, **2009**, 156, H588.

[25] Kudo, E. *et al.*,. *Thin Solid Films*, **2018**, 660, 730–732.

[26] Loka, C.; Yu, H. T.; and Lee, K. S. *Jpn. J. Appl. Phys.*, **2014**, 53, 08NE01-05.

[27] Gulen, M.; Yildirim, G.; Bal, S.; Varilci, A.; Belenli, I.; and Oz, M. *J. Mater. Sci. Mater. Electron.*, **2013**, 24, 467–474.

[28] Jeong, J.-A.; Kim, H.-K.; Koo, H.-W.; and Kim, T.-W. *Appl. Phys. Lett.*, **2013**, 103, 11902.

[29] Cho, E. N.; Moon, P.; Kim, C. E.; and Yun, I. *Expert Syst. Appl.*, **2012**, 39, 8885–8889.

[30] Roh, H. S.; Cho, S. H.; and Lee, W. J. *Phys. Status Solidi Appl. Mater. Sci.*, **2010**, 207, 1558–1562.

[31] Kim, H.; Lee, H.; Kal, J.; Hahn, J.; Kim, H.-K. AIP Advances. **2015**, 5, 107236.

[32] Balasundaraprabhu, R.; Monakhov, E. V.; Muthukumarasamy, N.; Nilsen, O.; and Svensson, B. G. *Mater. Chem. Phys.*, **2009**, 114, 425–429.

[33] Liu, W.-S. *et al.*,. *Appl. Surf. Sci.*, **2015**, 354, 31–35.

[34] Ali, A. H.; Shuhaimi, A.; and Hassan, Z. *Appl. Surf. Sci.*, **2014**, 288, 599–603.

[35] Zhao, X.; Li, H.; Yang, K.; Jiang, S.; Jiang, H.; and Zhang, W. *J. Alloys Compd.*, **2017**, 698, 147–151.

[36] Ghorannevis, Z.; Akbarnejad, E.; and Ghoranneviss, M. *J. Theor. Appl. Phys.*, **2015**, 9, 285–290.

[37] Guillén, C.; and Herrero, J. *J. Appl. Phys.*, **2007**, 101, 73514.

[38] Haacke, G. *J. Appl. Phys.*, **1976**, 47, 4086–4089.